Rainfall detection on a tropical island using a communication satellite downlink signal and artificial intelligence models

Raden Yudha Mardyansyah[1,2], Budhy Kurniawan[2], Santoso Soekirno[2], Danang Eko Nuryanto[4], Ferry Budhi Susetyo[3]
[1]Communication Network Center, Badan Meteorologi Klimatologi dan Geofisika, Jakarta, Indonesia
[2]Department of Physics, Faculty of Mathematics and Natural Sciences, Universitas Indonesia, Depok, Indonesia
[3]Department of Mechanical Engineering, Faculty of Engineering, Universitas Negeri Jakarta, Jakarta, Indonesia
[4]Research and Development Center, Badan Meteorologi Klimatologi dan Geofisika, Jakarta, Indonesia

Article Info

Article history:

Received Jan 26, 2026
Revised Jun 25, 2026
Accepted Jun 30, 2026

Keywords:

Deep learning
Ku-band satellite link
long-term performance
Machine learning
Satellite communication
Season-based evaluation

ABSTRACT

The development of rainfall estimates based on satellite links in several high latitude regions shows good results. However, its development for tropical regions is still very less promising, leaving the question of which method is worth using. In this work, we investigate artificial intelligence (AI) models by utilizing the Ku-band satellite downlink signal for rainfall detection on a tropical island. Long-term evaluation of all the models is performed using one year of rainfall intensity data. The findings of this study demonstrate that one-dimensional convolution neural network (1DCNN), long short-term memory (LSTM), and random forest (RF) models can effectively identify rainfall occurrences on tropical islands, with the area under the receiver operating characteristic curve (ROC) value of 0.84, 0.84, and 0.83, respectively. These three models consistently provide better accuracy in detecting the region's diverse rainfall patterns throughout the year. The 1DCNN has better performance compared to the other models, achieving accuracy values of 0.76 and 0.82 during the periods of lowest and highest rainfall, respectively. Considering the presence of numerous potential mislabeled rain samples in the dataset, this result is excellent. In addition, the utilization of higher resolution rainfall intensity data can be a great potential for real-time rainfall monitoring in the tropical region.

Corresponding Author:

Budhy Kurniawan
Department of Physics, Faculty of Mathematics and Natural Sciences, Universitas Indonesia
Building F, Universitas Indonesia Campus, Depok 16424, West Java, Indonesia
Email: budhy.kurniawan@sci.ui.ac.id

1. INTRODUCTION

Several studies have been conducted over the past 10 years on the use of telecommunications satellites' channel signals operating in the microwave frequency range [1] in the Ku (12–18 GHz) and Ka (27–40 GHz) frequency bands [2] as alternatives to rainfall measurements. The transmission of electromagnetic waves in these frequency ranges can be considerably affected by rain attenuation, as well as other effects caused by air gases and clouds, although these effects are less significant but more frequent. The reduction in the strength of the received signal is directly proportional to the quantity of precipitation encountered along the path of the wave [3].

Numerous researchers have investigated rainfall measurement from satellite link signals using both the power-law calculation [4] and artificial intelligence (AI) models [5]. Adirosi *et al.* [6] demonstrated that real-time rainfall intensity can be estimated from the attenuation of Ku- and Ka-band satellite reception signals by using the power-law model and rain cloud height data. Several additional satellite frequencies, including K-band [7], [8], X-band [9], and Q/V-band [10] have also been used. Researchers have constructed a system for the detection and estimation of rainfall fields from digital video broadcasting satellite receivers as part of the network for rain forecasting using broadband satellite telecommunications (NEFOCAST) and innovative satellite-based rainfall detection and estimation for rain (INSIDERAIN) Project in Italy, aimed at achieving regional coverage [11]–[14]. Rainfall intensity per minute in an inversion model for long-term (i.e., one year) performance has also been evaluated; this measurement was taken with a Ku-band satellite receiver built in Nanjing, China [15]. Gharanjik *et al.* [7] used an artificial neural network (ANN) to discern between rain and dry events by analyzing the carrier-to-noise power ratio data from the forward link and return link of a broadband satellite communication network in Betzdorf, Luxembourg. Recent research on rainfall detection in Nanjing, China, has used a support vector machine (SVM) to identify rainy and non-rainy periods with Ku-band satellite link signals [16].

The development of rainfall estimates based on satellite links in several high latitude regions shows good results. However, its development for tropical regions is still very less promising, leaving the question of which method is worth using. In this research, we will study AI models that have been used at high latitudes plus three other models which are expected to provide better performances. The long-term evaluation of all the models is also performed based on one year of rainfall intensity data.

2. METHOD

In this work, we examine one-dimensional convolution neural network (1DCNN), long short-term memory (LSTM), and random forest (RF) binary classification models that have never before been applied to the detection of rainfall from satellite downlink signals. The SVM and a multilayer perceptron (multilayer perceptron/MLP, a multi-layer ANN) are evaluated as comparison models. Figures 1(a) and (b) illustrates the architectural concept of the 1DCNN and LSTM models.

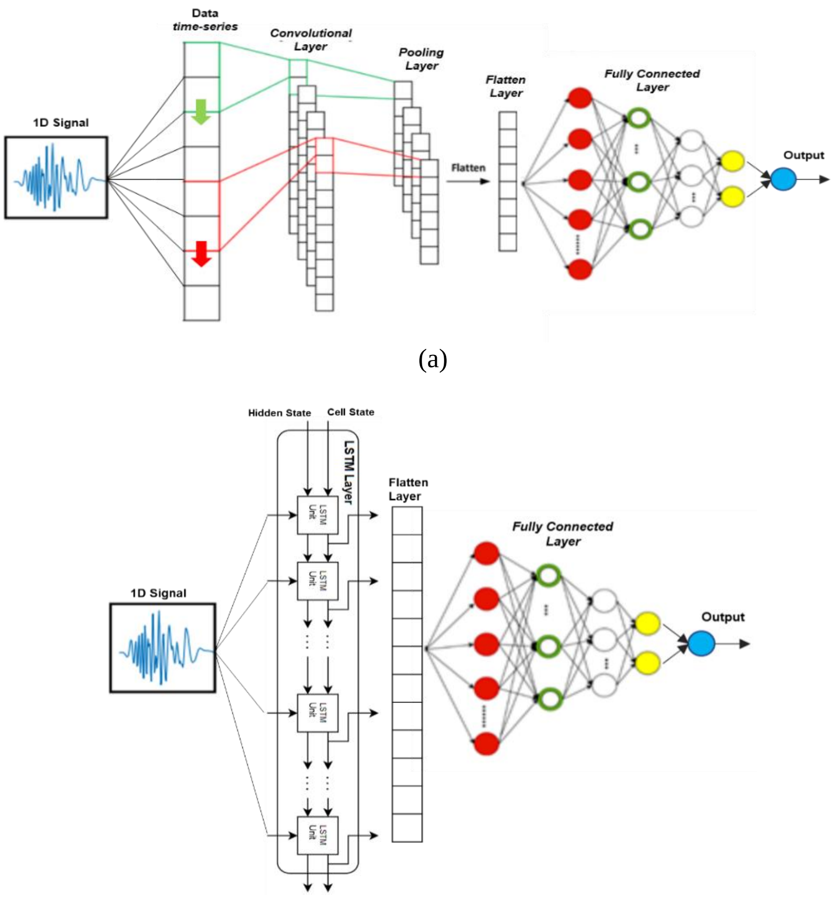

(a)

(b)

Figure 1. The architecture of (a) 1DCNN and (b) and LSTM

The 1DCNN is a specialized type of convolution neural network (CNN) [17] used for processing one-dimensional data, like sequences or time series. It employs convolutional layers with filters to capture local patterns and features in the input data. As depicted in Figure 1(a), 1DCNN consists of convolutional layer, pooling layer, dense layer and output layer which acts as the prediction output of the model. The LSTM model, proposed by Hochreiter and Schmidhuber [18], is a robust recurrent neural system specifically engineered to address the issues of exploding or vanishing gradients that commonly occur during the learning of long-term dependencies. Like the 1DCNN, the LSTM model is composed of a layer of LSTM units, a dense layer, and an output layer that serves as the model's prediction output, as depicted in Figure 1(b). The LSTM architecture comprises a collection of interconnected sub-networks, referred to as memory blocks or LSTM units. The purpose of the memory block is to preserve its state over time and control the flow of information through non-linear gating units. The transport of information to the next cell involves two states: the cell state and the hidden state. The hidden state at time step t encompasses the output of the LSTM layer for this specific time step. The cell state encompasses knowledge acquired from preceding time steps. During each time step, the layer either incorporates new information into the cell state or eliminates existing information from it.

The RF technique is an ensemble algorithm first introduced by Breiman [19]. It has been designed to handle various nonlinear classification and regression tasks. The bootstrap sampling method and random feature selection were used to create a large and diverse forest consisting of numerous decision trees [20]. RF outperforms a single decision tree and mitigates over-fitting by employing an averaging technique. The instability of decision trees is attributed to their high variation and low bias. The final result is determined by either selecting the category with the highest number of votes in the classification model or calculating the average prediction from all decision trees in the regression model. Significantly, it facilitates rapid processing for extensively parallel computing on substantial datasets or training multidimensional vectors with a high level of predictive accuracy.

2.1. Dataset

The models employed in this study utilize data on the energy per symbol to noise power spectral density ratio (Es/No) acquired over a period of one hour. This data represents the quality of the satellite signal received by the user terminal (UT) in a multi-spot-beam satellite network, as depicted in Figure 2 [21]. Numerous UTs are dispersed across specific satellite beam points and are connected to one or more network gateways, which serve as the network's communication hub. Each UT receives Ku-band downlink signals from Apstar-5C's 138 east orbital position. Since the Gateway satellite network employs a site diversity system [22], as postulated by Gharanjik *et al.* [7], the Es/No data received by the UT is dominated by rain on the downlink side from the satellite to the UT.

Each UT has a path to the internet at the network gateway for client access. In addition, a network management system (NMS) serves as a data traffic controller and collects the Es/No data received by each UT at the gateway location. The Es/No data for a specific period of time is stored in a database. By using hourly rainfall intensity data from the nearest Hellmann rain gauge (RG) [23], [24] at the Ranai Meteorological Station, each hour of Es/No data is classified as either rain or dry conditions. The Ranai Meteorological Station is a weather observation facility that is under the ownership of the Meteorological Climatological and Geophysical Agency of Indonesia. The rainfall intensity data from Hellmann's has undergone quality control due to the membership of the Ranai Meteorological Station in the Global Basic Observing Network of the World Meteorological Organization (WMO). The WMO Integrated Global Observing System (WIGOS) Station Identifier of Ranai Meteorological Station is 0-20000-0-96147 (https://oscar.wmo.int/surface/#/).

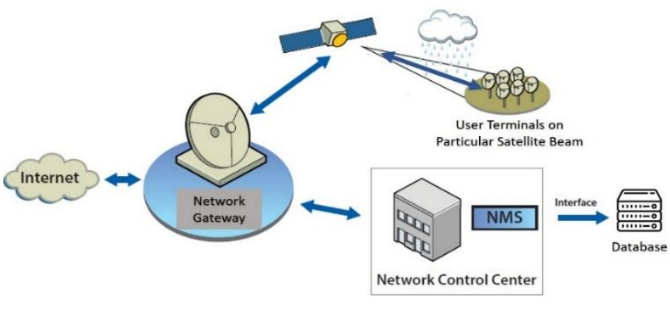

Figure 2. Ku-band satellite communication network

In Figure 3, the UT and RG are located on Natuna Island, which is a tropical island located in the South China Sea inside the Indonesian territory. The red line indicates the direction of the link between the UT and the satellite. The UT is part of the high-throughput-satellite broadband network operated by Telkomsat, a subsidiary of Telkom that provides satellite services in Indonesia. The company specializes in providing high-quality and international-standard upstream to downstream services.

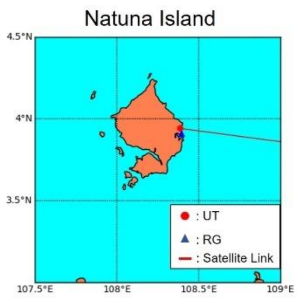

Figure 3. Location of the UT and RG on Natuna Island

Every two minutes, the network gateway stores the Es/No data sent by the UT in the database. The RG (3.912034°N, 108.393530°E), located 3.3 kilometers away from the UT (3.941110°N, 108.387666°E), measures rainfall intensity or rain rate (RR) in millimeters per hour. Based on several mesoscale cloud studies in Indonesia [25], [26], the location of the RG is considered to represent rainfall at the UT site because the former is found in the same wet region during extreme weather events. The UT and the RG are also situated in the same coastal region, which ensures that the World Meteorological Organization's recommended network coverage for rain gauges is maintained [27].

We define the Es/No parameter with dry or rain labels based on the rainfall intensity data, where RR > 0 denotes a rain label. Figure 4(a) shows the Es/No and RR data from December 2019 to September 2022. Each hour of Es/No data that corresponds to RR > 0 is highlighted in green in Figure 4(b) and represents a rain label; otherwise, it represents a dry label. The one-hour sample of Es/No data, denoted as $x_n = [\bar{x}$n-1, $\bar{x}$n-2, $\bar{x}$n-3, ... $\bar{x}$n-30], is formed by concatenating two-minute Es/No data into a single vector representing a time frame of one hour, according to the method used by Habi and Messer [28].

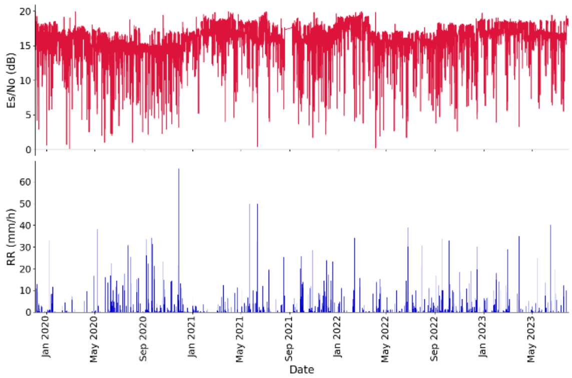

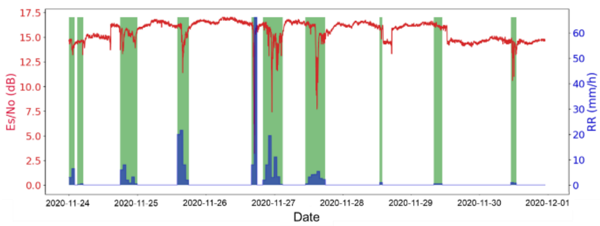

(a) (b)

Figure 4. Dataset of the Es/No in decibels (dB) and RR in millimeters per hour (mm/h); (a) from December 2019 through September 2022 and (b) sample data illustrating Es/No markings for both dry and rain conditions

2.2. Preprocessing

Figure 5 presents the flow chart of the rainfall detection model, which comprises three stages: (i) data preprocessing, (ii) model construction, and (iii) model evaluation. The initial step in data preprocessing involves the utilization of linear interpolation on Es/No data to address the gaps that arise due to the absence of a satellite connection link. Subsequently, data normalization is carried out, a procedure that has been explored by several authors [29], [30]. Interpolation is limited to data gaps of up to six minutes. As part of the normalization process, the subtraction of the median value derived from the entirety of the preceding and following 12-hour data is conducted for every time step. This method is implemented to optimize the performance of the model that will be employed. After interpolating and excluding all the missing values, there are a total of 22,456 samples.

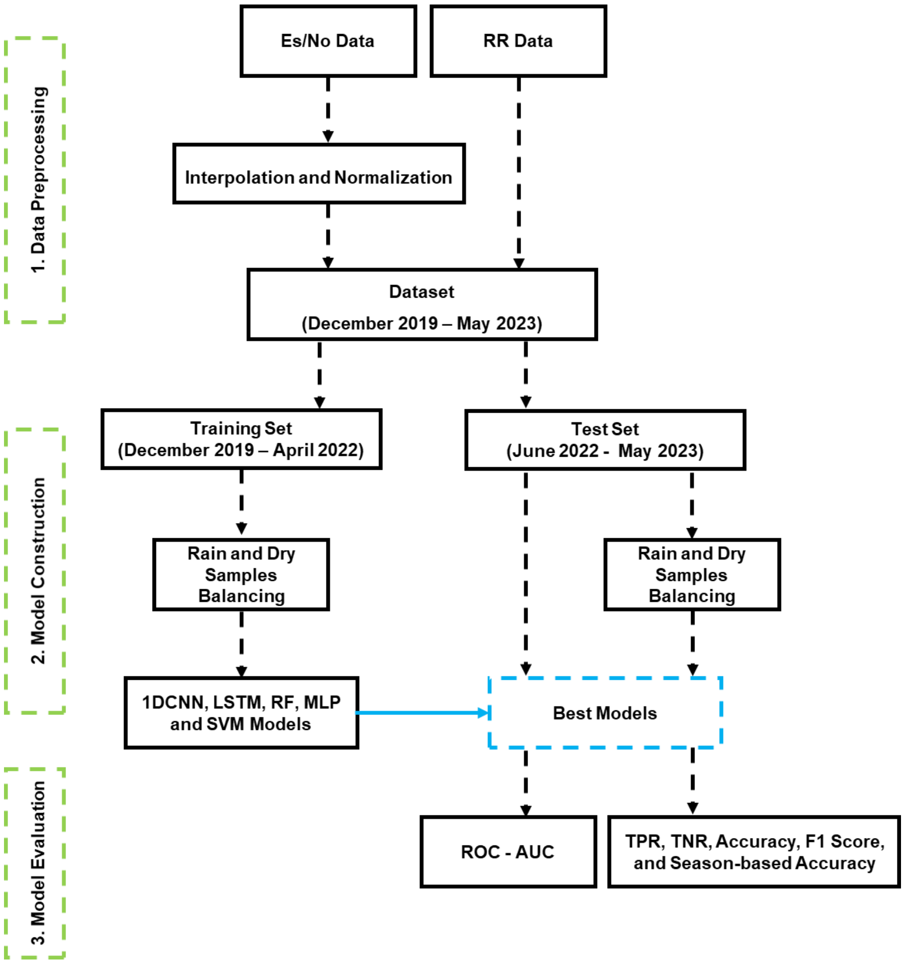

Figure 5. Flow chart of the rainfall detection model

After interpolation and normalization, the dataset is divided into training and testing sets. The model is trained with datasets ranging from December 2019 to April 2022. For long-term performance evaluation, we employ data from June 2022 to May 2023 in model testing. Drawing on Habi and Messer [28], we balance the rain and dry classes in both the training and testing datasets to enhance model performance. By randomly reducing the number of dry samples to match the number of rain samples, the undersampling approach is used to acquire an equalized (50:50) class ratio. In the end, the dataset consists of 3,046 training samples and 480 testing samples. During the training of the 1DCNN, MLP, and LSTM models, a random selection of 20% of the training data was allocated for data validation purposes. This subset of data was utilized to assess the performance and progress of the models throughout the training process.

2.3. Binary classification model

In this study, we examine the performance of five AI models for binary classification. The 1DCNN employs Polz *et al.*'s configuration [29] for microwave-link rain detection research. The MLP is employed by using dense layers derived from the 1DCNN. The LSTM model incorporates the layer introduced by Habi and Messer [28], employing the same amount of dense layers as the MLP. Table 1 presents the layer configuration for the 1DCNN, LSTM, and MLP models.

Table 1. Layer configuration for the 1DCNN, LSTM, and MLP models

	1DCNN		MLP		LSTM	
	Layer	Activation	Layer	Activation	Layer	Activation
Layer configuration	Conv 1D (24,3)	Relu	-	-	-	-
	Conv 1D (24,3)	Relu	-	-	-	-
	Max Pool 1D	-	-	-	-	-
	Conv 1D (48,3)	Relu	-	-	-	-
	Conv 1D (48,3)	Relu	-	-	-	-
	Max Pool 1D	-	-	-	-	-
	Conv 1D (48,3)	Relu	-	-	-	-
	Conv 1D (48,3)	Relu	-	-	-	-
	Max Pool 1D	-	-	-	-	-
	Flatten	-	-	-	LSTM (128)	Relu
	Dense (64)	Relu	Dense (64)	Relu	Dense (64)	Relu
	Dropout (0.4)	-	Dropout (0.4)	-	Dropout (0.4)	-
	Dense (64)	Relu	Dense (64)	Relu	Dense (64)	Relu
	Dropout (0.4)	-	Dropout (0.4)	-	Dropout (0.4)	-
	Dense (1)	Sigmoid	Dense (1)	Sigmoid	Dense (1)	Sigmoid
Optimizer	SGD (learning_rat e= 0.006)		SGD (learning_rate = 0.005)		Adam (learning_rate = 0.001)	

For the SVM and RF models, the default parameters are applied. Although SVM and RF are not classified as deep neural network techniques, they are commonly used for handling time series data and binary classification models [31]–[34]. The process for achieving the best rainfall detection for each model is illustrated in stage 2 of Figure 5. We train the 1DCNN, MLP, and LSTM models by using a batch size of four for a maximum of 1,000 epochs, with validation loss monitoring based on early stopping. The training process for each model involves numerous iterations, wherein the training data (specifically, the selection of dry samples) is randomized in various ways. This randomization is performed repeatedly until the best results are obtained. All the models are evaluated with the same set of test data.

2.4. Model evaluation

The final stage of Figure 5 involved the evaluation of each model in this study. The long-term evaluation of each classification model yields predictions that are subsequently compared with actual reference points. The outcome is a confusion matrix comprising true positives (TP), false positives (FP), false negatives (FN), and true negatives (TN), as illustrated in Table 2. Moreover, the outcomes of the confusion matrix are utilized to calculate evaluation metrics such as the true positive rate (TPR), the true negative rate (TNR), the overall accuracy, and the F1 score for predicting rain, as defined in Table 3.

Table 2. Confusion matrix of binary classification models

		Prediction	
		Dry	Rain
Actual	Dry	TN: predicted dry, actual dry	FP: predicted rain, actual dry
	Rain	FN: predicted dry, actual rain	TP: predicted rain, actual rain

Table 3. Evaluation metrics equations

Metrics	Equations
TPR	$\frac{TP}{TP + FN}$
TNR	$\frac{TN}{TN + FP}$
Accuracy	$\frac{TP + TN}{TP + TN + FP + FN}$
F1 score	$\frac{2TP}{2TP + FP + FN}$

In addition to the aforementioned evaluation metrics, the receiver operating characteristic (ROC) curve and the area under the curve (AUC) graphs are also utilized to depict the performance of individual binary classification models [35]. The evaluation encompasses all one-year test data as the ROC curve is unaffected by the ratio of dry and rain periods [29]. A perfect classifier will be located at the upper-left corner of the ROC space, which is at the coordinates (0, 1). In the context of classification, the AUC metric indicates the likelihood of a classifier correctly ranking a randomly chosen positive instance above a randomly chosen negative instance.

As a final evaluation, the models' consistency of performance in detecting diverse rainfall patterns is evaluated on a seasonal basis, in accordance with the climatology of Natuna Island [36], [37]. The periods examined are December to February (DJF), March to May (MAM), June to August (JJA), and September to November (SON) [38]. This evaluation aims to examine the consistency of the models' performances across a variety of rainfall patterns in one year.

3. RESULTS AND DISCUSSION

We evaluate the performance of all the models by using RR data samples from June 2022 to May 2023, as shown in Figure 6. These samples have various amounts and intensities of rain events for each season. Figure 6(a) presents 2,029 samples of 139 rain events with a maximum intensity of 39 mm/h, which were collected between June and August 2022. Figure 6(b) depicts 2,043 samples of 218 rain events with a maximum intensity of 33.7 mm/h from September to November 2022. Figure 6(c) shows 2,070 samples of 314 rain events with a maximum intensity of 30 mm/h from December 2022 to February 2023. Figure 6(d) presents 2,080 samples of 109 rain events with a maximum intensity of 35 mm/h from March to May 2023. There are a total of 780 rain events in the 8,222 samples used to evaluate the models.

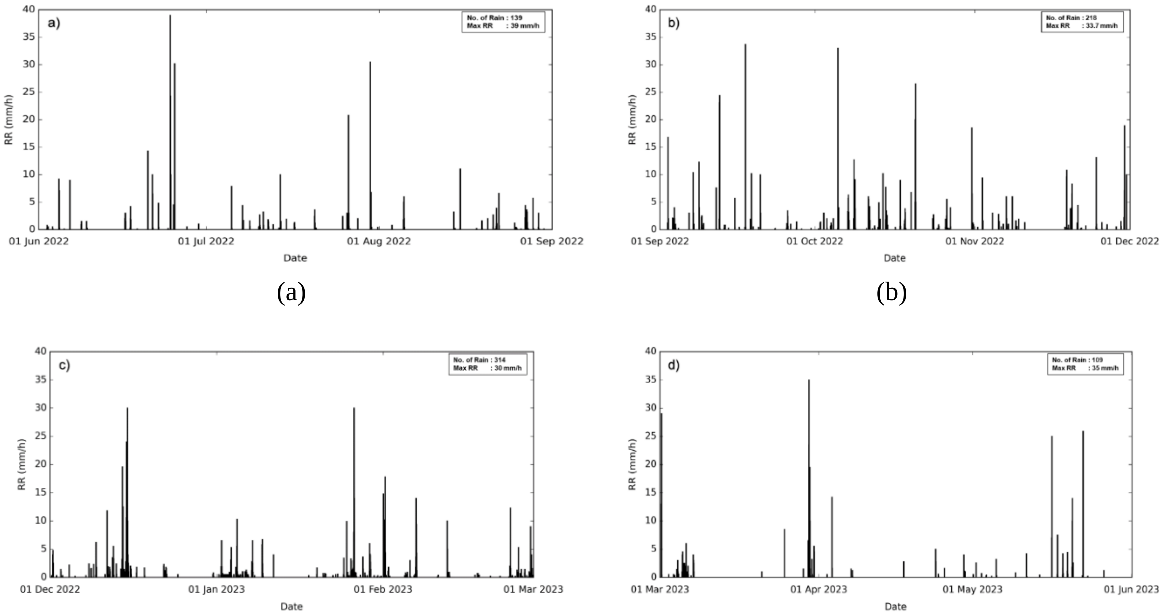

(a) (b) (c) (d)

Figure 6. Samples of rainfall intensity for long-term model evaluation; (a) June–August 2022, (b) September–November 2022, (c) December 2022–February 2023, and (d) March–May 2023

The evaluation of the binary classification model's performance is initially assessed through the utilization of the ROC curve, which incorporates various threshold values. This is illustrated in Figure 7. ROC graphs are graphical representations that depict the relationship between the TPR and the false positive rate (FPR). These graphs are two-dimensional, with the TPR represented on the y-axis and the FPR plotted on the x-axis. The TPR, also known as the hit rate or recall rate, represents the proportion of correctly predicted occurrences of rain in relation to the overall number of rainy events. Conversely, the FPR, often referred to as the false alarm rate, indicates the ratio of incorrectly predicted dry events to the total dry amount. The AUC describes predictive performance across all the possible classification thresholds. With the exception of the SVM model, all the models demonstrate excellent performance as binary classifiers in rain detection. This is evident from the convex shape of the ROC graphs and the AUC values, which exceed 0.8 [39], [40]. The AUC values for the 1DCNN, LSTM, RF, MLP, and SVM are 0.84, 0.84, 0.83, 0.82, and 0.79, respectively.

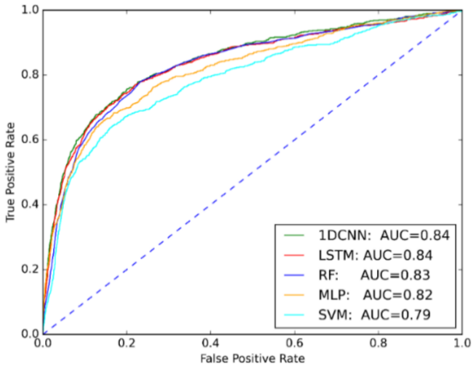

Figure 7. The ROC-AUC graph of model performance

The evaluation of the binary classification model's performance is initially assessed through the utilization of the ROC curve, which incorporates various threshold values. This is illustrated in Figure 7. ROC graphs are graphical representations that depict the relationship between the TPR and the FPR. These graphs are two-dimensional, with the TPR represented on the y-axis and the FPR plotted on the x-axis. The TPR, also known as the hit rate or recall rate, represents the proportion of correctly predicted occurrences of rain in relation to the overall number of rainy events. Conversely, the FPR, often referred to as the false alarm rate, indicates the ratio of incorrectly predicted dry events to the total dry amount. The AUC describes predictive performance across all the possible classification thresholds. With the exception of the SVM model, all the models demonstrate excellent performance as binary classifiers in rain detection. This is evident from the convex shape of the ROC graphs and the AUC values, which exceed 0.8 [39], [40]. The AUC values for the 1DCNN, LSTM, RF, MLP, and SVM are 0.84, 0.84, 0.83, 0.82, and 0.79, respectively.

In order to evaluate the TPR, TNR, accuracy, and F1 score, it is required to balance the test data by randomly reducing the number of dry samples to match the number of rain samples. Figure 8 presents the long-term evaluation metrics for all the models with a threshold of 0.5. Overall, all the models deliver more accurate predictions of dry conditions than rain conditions, as indicated by the fact that the TNR values exceed the TPR ones. This result is in line with research conducted by Polz *et al.* [29]. Three models; the 1DCNN, LSTM, and RF can detect rain better than the rest according to the TPR values. On average, 29% of rainfall events are incorrectly detected by the LSTM, 32% by the 1DCNN, and 33% by the RF, whereas the MLP and SVM incorrectly detect 47% and 52% of rain events, respectively.

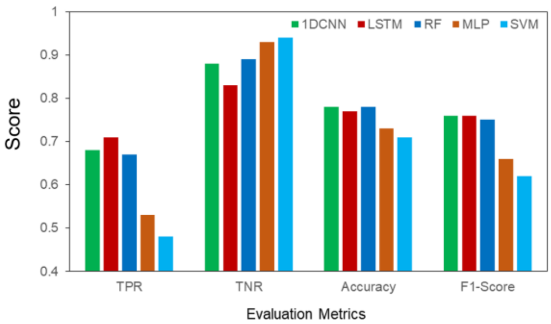

Figure 8. Evaluation metrics for all the models

Accuracy and F1 score are further aspects of evaluation. In terms of accuracy performance, the 1DCNN, RF, and LSTM models outperform the MLP and SVM with an accuracy range of 0.77–0.78, which is higher than the values for the MLP (0.73) and the SVM (0.71). Calculating the weighted average of a model's accuracy (also known as positive predictive value) and recall (i.e., sensitivity) yields the F1 score. In other words, the F1 score takes into account FP (actual dry but predicted rain) and FN (actual rain but predicted dry) and more accurately reflects the performance of a binary classification model. Again, the 1DCNN, LSTM, and RF models outperform the other models in detecting rain, with F1 scores ranging from 0.75 to 0.76, whereas the F1 scores of the MLP and the SVM are 0.66 and 0.62, respectively.

As a final performance evaluation, the accuracy of each model is tested on a seasonal basis. This evaluation is conducted to examine the consistency of the models' performances in detecting diverse rainfall patterns. Figure 9 shows the performances of the examined models during the JJA, SON, DJF, and MAM periods. All the models have higher performances in MAM because the number of rain events in the test data for this period is the lowest compared to the other periods. According to the results of this evaluation, the 1DCNN, LSTM, and RF consistently outperform the MLP and SVM, which have been employed in previous studies [7], [16]. In the DJF and MAM periods, where the number of rain events is highest and lowest, respectively, the 1DCNN outperforms the LSTM and RF with accuracy values of 0.76 in DJF and 0.82 in MAM.

In general, the performance of 1DCNN, LSTM, and RF, which we propose as binary classification models for rainfall detection, outperform the MLP and SVM as depicted in Table 4. The findings of this study demonstrate that 1DCNN, LSTM, and RF models can effectively identify rainfall occurrences on tropical islands. The RF model has a detection probability of 83%, whereas both 1DCNN and LSTM models have a detection probability of 84% each. Considering the presence of numerous potential mislabeled rain samples in the dataset, this result is excellent. This discrepancy is attributed to the significant distance between UT and RG, resulting in a likelihood of several rain occurrences that differ between the two sites. Furthermore, the performance of the RF is reliable and competitive when compared to the 1DCNN and the LSTM, despite the fact that default parameters are used.

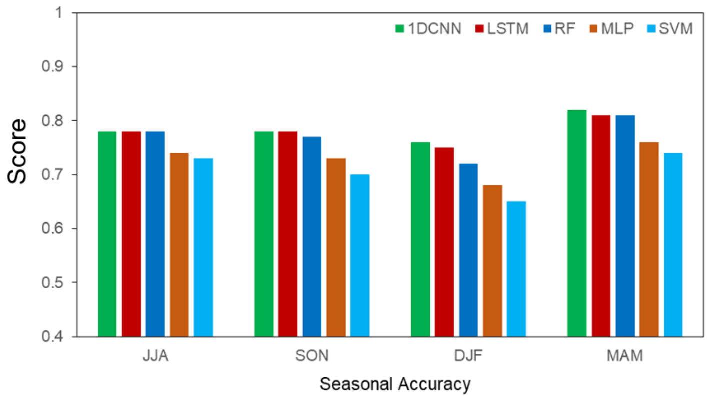

Figure 9. Seasonal accuracy performance of the models

Table 4. Comparison of models' performance

Model	AUC	Accuracy	F1-score	Long-term accuracy			
				JJA	SON	DJF	MAM
1DCNN	0.84	0.78	0.76	0.78	0.78	0.76	0.82
LSTM	0.84	0.77	0.76	0.78	0.78	0.75	0.81
RF	0.83	0.78	0.75	0.78	0.77	0.72	0.81
MLP	0.82	0.73	0.66	0.74	0.73	0.68	0.76
SVM	0.79	0.71	0.62	0.73	0.70	0.65	0.74

4. CONCLUSION

In this article, we investigate AI techniques based on binary classification to detect rain from Ku-band communication satellite downlink signals. The study area is located on the Indonesian Island of Natuna, which is in the tropical equatorial region. Our research demonstrates that satellite downlink signals can detect rainfall on a tropical island. The results of this study indicate that 1DCNN, LSTM, and RF models are capable of accurately detecting rainfall events, with a detection rate of up to 84%. Furthermore, each model provides consistency of performance with better accuracy in detecting the region's diverse rainfall patterns throughout the year. In the DJF and MAM periods, when the number of rain events is highest and lowest, respectively, the 1DCNN outperforms all the other models with accuracy values of 0.76 in DJF and 0.82 in MAM. These findings confirm that the use of AI models for rainfall detection using satellite link signals is promising for tropical regions. Considering the errors in rain-dry labeling in both the training and test data, this result is excellent. Future research is expected to use the UT and RG at the same location to improve the models' accuracy. In addition, the utilization of higher resolution rainfall intensity data can be a great potential for real-time rainfall monitoring in the tropical region.

ACKNOWLEDGEMENTS

The research is supported by Badan Riset dan Inovasi Nasional's Degree by Research program. Badan Meteorologi Klimatologi dan Geofisika dan PT. Telkomsat Indonesia are also thanked for supplying the data.

FUNDING INFORMATION

The authors wish to express their appreciation to Kemendikbudristek of Republik Indonesia for the financial support of Hibah Penelitian Disertasi Doktor no. NKB-1131/UN2.RST/HKP.05.00/2023.

AUTHOR CONTRIBUTIONS STATEMENT

This journal uses the Contributor Roles Taxonomy (CRediT) to recognize individual author contributions, reduce authorship disputes, and facilitate collaboration.

Name of Author	C	M	So	Va	Fo	I	R	D	O	E	Vi	Su	P	Fu
Raden Yudha Mardyansyah	✓	✓	✓	✓	✓	✓	✓	✓	✓	✓	✓			
Budhy Kurniawan	✓									✓		✓	✓	✓
Santoso Soekirno	✓									✓		✓		✓
Danang Eko Nuryanto	✓	✓			✓					✓		✓		
Ferry Budhi Susetyo					✓					✓		✓		

C : **C**onceptualization
M : **M**ethodology
So : **So**ftware
Va : **Va**lidation
Fo : **Fo**rmal analysis
I : **I**nvestigation
R : **R**esources
D : **D**ata Curation
O : Writing - **O**riginal Draft
E : Writing - Review & **E**diting
Vi : **Vi**sualization
Su : **Su**pervision
P : **P**roject administration
Fu : **Fu**nding acquisition

CONFLICT OF INTEREST STATEMENT

The authors state no conflict of interest.

DATA AVAILABILITY

The data that support the findings of this study are available from the corresponding author, R.Y.M., upon reasonable request.

REFERENCES

[1] R. T. Hitchcock, "Radio-Frequency and Microwave Radiation," *Patty's Toxicology. Wiley*, pp. 133–168, Aug. 17, 2012. doi: 10.1002/0471435139.tox101.pub2.
[2] IEEE, "IEEE Standard Letter Designations for Radar-Frequency Bands," 2002. doi: 10.1109/IEEESTD.2003.94224.
[3] G. J. G. Upton, A. R. Holt, R. J. Cummings, A. R. Rahimi, and J. W. F. Goddard, "Microwave links: The future for urban rainfall measurement?," *Atmospheric Research*, vol. 77, no. 1-4 SPEC. ISS., pp. 300–312, 2005, doi: 10.1016/j.atmosres.2004.10.009.
[4] R. Olsen, D. Rogers, and D. Hodge, "The aRb relation in the calculation of rain attenuation," *IEEE Transactions on Antennas and Propagation*, vol. 26, no. 2, pp. 318–329, 1978, doi: 10.1109/TAP.1978.1141845.
[5] A. H. Marblestone, G. Wayne, and K. P. Kording, "Toward an Integration of Deep Learning and Neuroscience," *Frontiers in Computational Neuroscience*, vol. 10, 2016, doi: 10.3389/fncom.2016.00094.
[6] E. Adirosi *et al.*, "Exploiting satellite Ka and Ku links for the real-time estimation of rain intensity," in *2017 32nd General Assembly and Scientific Symposium of the International Union of Radio Science, URSI GASS 2017*, 2017, vol. 2017-Janua, pp. 1–4, doi: 10.23919/URSIGASS.2017.8105128.
[7] A. Gharanjik, M. R. Bhavani Shankar, F. Zimmer, and B. Ottersten, "Centralized rainfall estimation using carrier to noise of satellite communication links," *IEEE Journal on Selected Areas in Communications*, vol. 36, no. 5, pp. 1065–1073, 2018, doi: 10.1109/JSAC.2018.2832798.
[8] A. Gharanjik, K. V. Mishra, B. Shankar, and B. Ottersten, "Learning-based rainfall estimation via communication satellite links," in *2018 IEEE Statistical Signal Processing Workshop, SSP 2018*, 2018, pp. 115–119, doi: 10.1109/SSP.2018.8450726.
[9] L. Xu, X. Shen, D. D. Huang, X. Feng, and W. Wang, "Tomographic reconstruction of rainfall fields using satellite communication links," in *2017 23rd Asia-Pacific Conference on Communications (APCC)*, 2017, pp. 1–5, doi: 10.23919/APCC.2017.8303986.
[10] T. Rossi, M. De Sanctis, S. Di Domenico, M. Ruggieri, and E. Cianca, "Experimental Model of Rainfall Rate Estimation Through the Opportunistic Use of Q-/V-Band Satellite Links," *IEEE Transactions on Aerospace and Electronic Systems*, vol. 58, no. 5, pp. 3802–3809, 2022, doi: 10.1109/TAES.2022.3163128.
[11] E. Adirosi *et al.*, "Evaluation of rainfall Eestimation derived from commercial interactive DVB receivers using disdrometer, rain

Gauge, and weather radar," *IEEE Transactions on Geoscience and Remote Sensing*, vol. 59, no. 11, pp. 8978–8991, 2021, doi: 10.1109/TGRS.2020.3041448.

[12] S. Angeloni *et al.*, "Enhanced estimation of rainfall from opportunistic microwave satellite signals," *IEEE Transactions on Geoscience and Remote Sensing*, vol. 62, pp. 1–12, 2024, doi: 10.1109/TGRS.2023.3349100.

[13] F. Giannetti *et al.*, "Real-time rain rate evaluation via satellite downlink signal attenuation measurement," *Sensors*, vol. 17, no. 8, p. 1864, Aug. 2017, doi: 10.3390/s17081864.

[14] F. Giannetti, M. Moretti, R. Reggiannini, and A. Vaccaro, "The NEFOCAST system for detection and estimation of rainfall fields by the opportunistic use of broadcast satellite signals," *IEEE Aerospace and Electronic Systems Magazine*, vol. 34, no. 6, pp. 16–27, Jun. 2019, doi: 10.1109/MAES.2019.2916292.

[15] Y. Zhao, X. Liu, M. Xian, and T. Gao, "Statistical Study of Rainfall Inversion Using the Earth-Space Link at the Ku Band: Optimization and Validation for 1 Year of Data," *IEEE Journal of Selected Topics in Applied Earth Observations and Remote Sensing*, vol. 14, pp. 9486–9494, 2021, doi: 10.1109/JSTARS.2021.3111336.

[16] M. Xian, X. Liu, M. Yin, K. Song, S. Zhao, and T. Gao, "Rainfall Monitoring Based on Machine Learning by Earth-Space Link in the Ku Band," *IEEE Journal of Selected Topics in Applied Earth Observations and Remote Sensing*, vol. 13, pp. 3656–3668, 2020, doi: 10.1109/JSTARS.2020.3004375.

[17] S. Kiranyaz, O. Avci, O. Abdeljaber, T. Ince, M. Gabbouj, and D. J. Inman, "1D convolutional neural networks and applications: A survey," *Mechanical Systems and Signal Processing*, vol. 151, p. 107398, 2021, doi: 10.1016/j.ymssp.2020.107398.

[18] S. Hochreiter and J. Schmidhuber, "Long short-term memory," *Neural Computation*, vol. 9, no. 8, pp. 1735–1780, 1997, doi: 10.1162/neco.1997.9.8.1735.

[19] L. Breiman, "Random forests," *Machine Learning*, vol. 45, no. 1, pp. 5–32, Oct. 2001, doi: 10.1023/A:1010933404324.

[20] K. Gaurav, A. Kumar, P. Singh, A. Kumari, M. Kasar, and T. Suryawanshi, "Human disease prediction using machine learning techniques and real-life parameters," *International Journal of Engineering*, vol. 36, no. 6, pp. 1092–1098, 2023, doi: 10.5829/IJE.2023.36.06C.07.

[21] L. J. Ippolito, "High throughput satellites," in *Satellite Communications Systems Engineering*, Wiley, 2017, pp. 398–422.

[22] M. R. Islam, A. K. Lwas, and M. H. Habaebi, "Site diversity gain for earth-to-satellite links using rain intensity measurement," *Indonesian Journal of Electrical Engineering and Informatics*, vol. 5, no. 4, pp. 330–338, 2017, doi: 10.11591/ijeei.v5i4.364.

[23] R. M. Putra, A. Kurniawan, I. A. Rangga, M. Ryan, Endarwin, and A. Luthfi, "An Evaluation Graph of Hourly Rainfall Estimation in Malang," *IOP Conference Series: Earth and Environmental Science*, vol. 303, no. 1, 2019, doi: 10.1088/1755-1315/303/1/012031.

[24] M. Hoffmann, R. Schwartengräber, G. Wessolek, and A. Peters, "Comparison of simple rain gauge measurements with precision lysimeter data," *Atmospheric Research*, vol. 174–175, pp. 120–123, 2016, doi: 10.1016/j.atmosres.2016.01.016.

[25] N. S. Putri, T. Hayasaka, and K. D. Whitehall, "The Properties of Mesoscale Convective Systems in Indonesia Detected Using the Grab 'Em Tag 'Em Graph 'Em (GTG) Algorithm," *Journal of the Meteorological Society of Japan. Ser. II*, vol. 95, no. 6, pp. 391–409, 2017, doi: 10.2151/jmsj.2017-026.

[26] Trismidianto, E. Yulihastin, H. Satyawardhana, J. T. Nugroho, and S. Ishida, "The Contribution of the Mesoscale Convective Complexes (MCCs) to total rainfall over Indonesian Maritime Continent," *IOP Conference Series: Earth and Environmental Science*, vol. 54, p. 12027, 2017, doi: 10.1088/1755-1315/54/1/012027.

[27] WMO, *Guide to Hydrological Practices, Volume I. Hydrology – From measurement to hydrological information, 6th Edition*. 2008.

[28] H. V. Habi and H. Messer, "Wet-dry classification using LSTM and commercial microwave links," in *Proceedings of the IEEE Sensor Array and Multichannel Signal Processing Workshop*, 2018, vol. 2018-July, pp. 149–153, doi: 10.1109/SAM.2018.8448679.

[29] J. Polz, C. Chwala, M. Graf, and H. Kunstmann, "Rain event detection in commercial microwave link attenuation data using convolutional neural networks," *Atmospheric Measurement Techniques*, vol. 13, no. 7, pp. 3835–3853, 2020, doi: 10.5194/amt-13-3835-2020.

[30] K. K. Kumah, J. C. B. Hoedjes, N. David, B. H. P. Maathuis, H. O. Gao, and B. Z. Su, "Combining mwl and msg seviri satellite signals for rainfall detection and estimation," *Atmosphere*, vol. 11, no. 9, p. 884, 2020, doi: 10.3390/ATMOS11090884.

[31] F. Negaresh, M. Kaedi, and Z. Zojaji, "Gender Identification of Mobile Phone Users based on Internet Usage Pattern," *International Journal of Engineering*, vol. 36, no. 2, pp. 335–347, 2023, doi: 10.5829/ije.2023.36.02b.13.

[32] M. Gandomi and H. Hassanpour, "Behavioral analysis of traffic flow for an effective network traffic identification," *International Journal of Engineering, Transactions B: Applications*, vol. 30, no. 11, pp. 1740–1745, 2017.

[33] M. Khedmati, F. Seifi, and M. J. Azizi, "Time Series Forecasting of Bitcoin Price Based on Autoregressive Integrated Moving Average and Machine Learning Approaches," *International Journal of Engineering*, vol. 33, no. 7, pp. 1293–1303, 2020, doi: 10.5829/ije.2020.33.07a.16.

[34] V. Derbentsev, V. Babenko, K. Khrustalev, H. Obruch, and S. Khrustalova, "Comparative performance of machine learning ensemble algorithms for forecasting cryptocurrency prices," *International Journal of Engineering, Transactions A: Basics*, vol. 34, no. 1, pp. 140–148, 2021, doi: 10.5829/IJE.2021.34.01A.16.

[35] T. Fawcett, "An introduction to ROC analysis," *Pattern Recognition Letters*, vol. 27, no. 8, pp. 861–874, 2006, doi: 10.1016/j.patrec.2005.10.010.

[36] H. H. Hendon, "Indonesian rainfall variability: Impacts of ENSO and local air-sea interaction," *Journal of Climate*, vol. 16, no. 11, pp. 1775–1790, 2003, doi: 10.1175/1520-0442(2003)016<1775:IRVIOE>2.0.CO;2.

[37] R. Hafsaridewi, H. Hikmah, A. Zulham, P. A. Soejarwo, and B. V. I. Yanti, "Fishers' resilience towards extreme weather conditions in the South China Sea: a case study of Natuna Islands, Indonesia," *Omni-Akuatika*, vol. 16, no. 3, p. 49, Dec. 2020, doi: 10.20884/1.oa.2020.16.3.856.

[38] E. Aldrian and R. Dwi Susanto, "Identification of three dominant rainfall regions within Indonesia and their relationship to sea surface temperature," *International Journal of Climatology*, vol. 23, no. 12, pp. 1435–1452, 2003, doi: 10.1002/joc.950.

[39] F. Melo, "Area under the ROC Curve," *Encyclopedia of Systems Biology*. *Springer New York*, pp. 38–39, 2013. doi: 10.1007/978-1-4419-9863-7_209.

[40] G. Quek *et al.*, "Comparing performance of discomfort glare metrics in high and low adaptation levels," *Building and Environment*, vol. 206, p. 108335, 2021, doi: 10.1016/j.buildenv.2021.108335.

BIOGRAPHIES OF AUTHORS

Raden Yudha Mardyansyah is a Research Scientist at Meteorological, Climatological, and Geophysical Agency. His research focuses on machine learning methods, including one-dimensional convolutional neural networks and random forest models, for rainfall intensity estimation from Ku-band satellite communication signal attenuation fused with satellite remote-sensing data, with a focus on tropical Indonesian sites. His research interests include satellite communications, machine learning, and rainfall prediction. He can be contacted at email: yudha.mardyansyah@bmkg.go.id.

Budhy Kurniawan is a lecturer and researcher in the Department of Physics at Universitas Indonesia. His primary research focuses on magnetism and condensed matter physics, including magnetic materials, quantum spin systems, magnetoresistance, magnetocaloric effects, and the structural properties of thin films and perovskite manganites. He can be contacted at email: budhy.kurniawan@sci.ui.ac.id.

Santoso Soekirno holds a Ph.D. degree from the University of Besançon, France, and serves as a senior lecturer in the Department of Physics at Universitas Indonesia. His primary research interests center on sensors and electronics instrumentation, including transducer technologies, intelligent sensing systems, environmental monitoring (such as air quality and automatic weather stations), and smart electronic systems. He can be contacted at email: santoso.s@sci.ui.ac.id.

Danang Eko Nuryanto holds a Doctor of Philosophy (Ph.D.) degree and serves as a prominent researcher at the Center for Research and Development, Meteorological, Climatological, and Geophysical Agency (BMKG) in Jakarta, Indonesia. His primary research interests focus on meteorology, climatology, monsoon dynamics, mesoscale convective systems, numerical weather prediction modeling, and applied climate studies. He can be contacted at email: danang.eko@bmkg.go.id.

Ferry Budhi Susetyo received his Bachelor's degree in Mechanical Engineering from Universitas Pancasila and Universitas Lampung, followed by his Master's degree and Ph.D. in Materials Science from Universitas Indonesia. He is currently a lecturer in the Department of Mechanical Engineering, Faculty of Engineering at Universitas Negeri Jakarta (UNJ), Indonesia. His primary research interests include welding and material engineering, surface coatings, electrodeposition, corrosion behavior, and material characterization. He can be contacted at email: fbudhi@unj.ac.id.